

Journal of Sustainability for Energy

https://www.acadlore.com/journals/JSE



Promoting Effect of TiCl4 Pre-Coating Time on TiO₂ Semiconductors on Double Layer Dye-Sensitized Solar Cell

Zainal Arifin*, Suyitno, Syamsul Hadi, Singgih Dwi Prasetyo, Muhammad Hasbi

Department of Mechanical Engineering, Universitas Sebelas Maret, 57126 Surakarta, Indonesia

* Correspondence: Zainal Arifin (zainal arifin@staff.uns.ac.id)

Received: 11-13-2022 **Revised:** 11-30-2022 **Accepted:** 12-18-2022

Citation: Z. Arifin, Suyitno, S. Hadi, S. D. Prasetyo, and M. Hasbi, "Promoting effect of TiCl₄ pre-coating time on TiO₂ semiconductors on double layer dye-sensitized solar cell," *J. Sustain. Energy*, vol. 1, no. 1, pp. 18-26, 2022. https://doi.org/10.56578/jse010103.



© 2022 by the authors. Licensee Acadlore Publishing Services Limited, Hong Kong. This article can be downloaded for free, and reused and quoted with a citation of the original published version, under the CC BY 4.0 license.

Abstract: The invention of chemically flexible solar cells, known as dye-sensitive solar cells (DSSC), has led to cheaper, more ecologically friendly, yet inefficient solar cells. The poor link between the semiconductor and the substrate, which impacts the DSSC electrons' mobility, is the root reason of the low efficiency. TiCl₄ pre-coatings have been used in many studies on semiconductor engineering to boost electron mobility. In order to lower the internal resistance in the DSSC, it is known that using TiCl₄ pre-coating affects the mechanical strength between the semiconductor and the substrate. TiCl₄ pre-coating can be done by immersing FTO glass, where semiconductors have deposited, in the TiCl₄ solution. This study examines how the TiCl₄ pre-coating time in the production of TiO₂ semiconductors affects DSSC performance. To reveal the effects on alterations in the semiconductor morphology of TiO₂, immersion times in the TiCl₄ treatment were set to 10, 20, 30, 40, 50, and 60mins. The results show that TiO₂ nanoparticles with a 60min TiCl₄ treatment had better connectivity between individual particles than those with shorter treatments. The performance metrics like open circuit photovoltage (Voc), short-circuit photocurrent density (Jsc), and fill factor (FF), and efficiency (η) were 0.569 V, 7,616 mA/cm², 43.3%, and 2.208%, respectively.

Keywords: DSSC; TiCl₄ pre-coating; TiO₂ semiconductors; Morphology; Immersion time

1. Introduction

The potential of solar energy has piqued the interest of various scholars. Wasfi adopted solar cells to harness the power of the sun [1]. Solar energy can be captured using solar cells through a photovoltaic process. The electrons in the crystalline structure of a semiconductor material are released from their atomic bonds to form energy packets. These packets are used to create an electric current. Silicon cells have been used to create solar cells with success. Although silicon-based solar cells have an efficiency of about 18%, they are expensive and difficult to produce [2].

Gratzel created dye-sensitized solar cells, which are less expensive and environmentally benign solar cells with chemical flexibility (DSSC). The photocurrent voltage curve (IV curve), open circuit photovoltage (Voc), fill factor (FF), short-circuit photocurrent density (Jsc), and efficiency (η) are some of the measures to evaluate the performance of the DSSC. Substrates, semiconductors (photoanodes), dyes, electrolytes, and counter electrodes are the main components of DSSC [3, 4]. The efficiency of DSSC hinges on high electron mobility semiconductors with wide surface areas for dye absorption [5].

In the DSSC application, the semiconductor layer is used as a dye absorption material on each surface to provide electron excitation [6]. It is generally accepted that semiconductor nanoparticles have the highest surface area and are the best at optimally absorbing dye molecules. However, because the required connections for electrons are diminished and dispersed randomly, these structures decrease the mobility of electrons from one particle to another [7]. Materials such as Nickel (II) Oxide (NiO), Titanium Oxide (TiO₂), and Zinc Oxide (ZnO) make up DSSC semiconductors [8]. The great performance of the DSSC is attributed to semiconductor engineering, which is known to boost dye absorption and electron excitation by photons [9].

TiO₂ semiconductors are well suited for usage as nanoparticle coatings due to their excellence in electron

injection and great stability [10]. The ZnO nanofiber semiconductor, on the other hand, possesses the qualities of high electron mobility or transport rates as well as a wider energy bandgap value to convert more photon energy [11]. For optimum performance, double layer semiconductor engineering is often adopted: the DSSC is sandwiched between two layers of semiconductors. In this way, the DSSC can more effectively absorb and transform the photon energy. The efficiency of the DSSC can be greatly increased by the TiO₂ nanoparticle/ZnO nanofiber semiconductors [12].

Compared to ZnO semiconductors, TiO₂ semiconductors significantly improves DSSC performance [13-15]. Semiconductor TiO₂ nanoparticles, however, have weak adhesive bonding because of the limited connection between the particles. This leads to subpar DSSC performance [16, 17]. The type of adhesive bond between the semiconductor and the TCO (transparent conductive oxide) substrate determines the TiO₂ semiconductor performance in DSSC applications [18]. Increased mobility of oxidized electrons in the semiconductor, due to high adhesive qualities, might push up Jsc [19].

It is exciting to study the increase in adhesive bond, as it may enhance DSSC performance. By pre-coating the semiconductor and substrate, the researchers could successfully create the adhesive bond [20]. TiCl₄ is a promising material for pre-coating [21]. In general, semiconductor TCO glass can be immersed to pre-coat TiCl₄ on DSSC semiconductors [22, 23]. The internal resistance in the DSSC can be decreased thanks to the structure of TiCl₄, which is known to increase the mechanical strength between the semiconductor and the substrate [24]. The increased adhesion between the two can enhance Jsc [25]. This paper investigates the impact of TiCl₄ pre-coating time on the production of TiO₂ semiconductors for the TiO₂/ZnO double-layer DSSC.

2. Methodology

2.1 Semiconductor Preparation

In this study, the TCO substrate is a kind of fluorine-doped tin oxide (FTO) substrate, which has been doped with semiconductor TiO₂ nanoparticles. To maintain superior electrical conductivity and avoid electron and hole recombination, a large surface area, strong connections between the TiO₂ particles, and adequate adhesion between the TiO₂ layer and the TCO coated glass are essential [26, 27]. To demonstrate that this construct may operate as an active layer and scatter simultaneously to boost dye sensitization, electron transport rate, and ultimately cell efficiency, it is necessary to optimize the shape of the TiO₂ layer in accordance with the aforementioned parameters [28].

In practice, surface retardation can thwart electron recombination on the TiO₂ surface. Through the coadsorption of materials with dyes and the use of insulating layers and materials, modified TiO₂ surfaces have been created in numerous investigations [29-32]. One of the most popular modification techniques is TiCl₄ pre-coating, which has the ability to prevent electronic recombination [33]. The mechanical contact between the active layer and TCO, particle connection, electron transport coefficient, and ensuing power conversion efficiency were all enhanced by the TiCl₄ treatment [26].

In this study, the semiconductor is pre-coated with TiCl₄ using a 40 mM molar TiCl₄ solution. By combining 4 mL of TiCl₄ solution (Merck, 1 M) with 96 mL of distilled water, 40 mM of TiCl₄ solution was created. To disclose how TiCl₄ pre-coating affects the morphological structure of the semiconductor and the functionality of the DSSC, different immersion times (10, 20, 30, 40, 50, and 60mins) were adopted for the pre-coating process. The immersion time refers to the period that TiO₂ photoelectrodes are submerged in the coagulated dye solution [34].

Before the TiCl₄ treatment, the FTO glass, deposited with TiO₂, was rinsed with water and ethanol. Then, the FTO glass deposited with TiO₂ semiconductors was immersed in 20 mL of TiCl₄ solution at 70°C. After that, the glass was drained and rinsed with water and ethanol to remove the dirt, before being sintered at 500°C for 30min with a heating rate of 5°C/min.

TiO₂ nanoparticles/ZnO nanofibers with double-layer semiconductors are used in this study. Electrospinning was performed to create the ZnO nanofiber. The precursor solution was prepared with 10 mL distilled water and 1 g of PVA (Merck, MW = 72,000) (H₂O). The solution was stirred at 70°C for 4 h to homogenization, and then allowed to stand at room temperature for 8h. The Zn (Ac)2 solution was synthesized using 2 g zinc acetate dihydrate ((CH₃COO)2Zn.2H₂O, Merck) and 8 mL distilled water (H₂O). Next, the homogenization was carried out by stirring at 70°C for 1h. After that, the homogenization between the PVA solution and Zn (Ac)2 was carried out with a 4: 1 wt% at 70°C for 8h. Furthermore, the PVA/Zn (Ac)2 solution was allowed to stand at room temperature for 24h to remove the foams. In the end, the PVA/Zn (Ac)2 solution was obtained to produce the ZnO nanofibers, using an electrospinning machine [35].

One millimeter of injection pump electrospinning solution was filled with the synthesized solution. The collector plate of FTO glass, which has been coated with TiO₂ semiconductor nanoparticles through direct deposition, was linked to the negative terminal of a 15 kV high voltage at a distance of 8 cm horizontally from the syringe of the electrospinning solution pump.

The solution will be drawn to the electrostatic field on the negatively charged FTO glass collecting plate when

the solution is forced out and the tip of the needle where the solution exits has been exposed to high voltage. A flow rate of 4 L/min was employed to move the solution through the needle. The solution then pulls strands known as green fibers that adhere to the collecting plate's surface. To get rid of stuck-on dirt, the green fibers were then sintered at 500°C for an hour at a heating rate of 5°C/min. A double-layer semiconductor could thus be created by depositing nanofibers in FTO.

2.2 DSSC Fabrication and Testing

The FTO glass is submerged in N719 dye from diesel for 24h after the sintering process is complete, so that the dye can be thoroughly absorbed. The counter electrode is then joined with the FTO glass, and the electrolyte is injected through the counter electrode's hole. Iodide (I3-) EL-HPE from Dyesol was employed as the electrolyte solution.

Next, an SEM (Scanning Electron Microscope) test was carried out to determine the morphological structure of the semiconductor TiO₂ nanoparticles. Before electrospinning, a SEM examination is performed after the initial sintering process. To ascertain the impact of TiCl₄ pre-coating on the structural shape of semiconductor compounds, X-ray diffraction (XRD) tests were performed. The Uv-Vis test was utilized to determine the dye loading value, or how much dye the semiconductor can absorb. The Uv-Vis test yields the absorbance, which is used to determine the dye loading value using the Lambert-Beer formula:

$$A = \varepsilon. c. l \tag{1}$$

where, A is the absorbance intensity of the solution; ε is the extrinsic molar coefficient of the solution; c is the concentration of the solution; l is the length of the light path in the beam or cuvette.

The solar simulator test can be used to determine the DSSC performance. An IV curve will be generated from the solar simulator test, and this curve will then be used to generate other parameters like Jsc, Voc, FF, and η . When the solar cell electrodes are short-circuited together, a current known as Jsc flows via the external circuit. The voltage at which there is no current flowing through the external circuit is known as Voc. This is the highest voltage a solar cell can produce. The maximum power point (PMPP) on the current curve IV is the sum of the current and voltage. The FF is the ratio between the maximum power (PMPP) and the product between Isc and Voc:

$$FF = \frac{V_{MPP} \times I_{MPP}}{I_{SC} \times V_{OC}} \tag{2}$$

Finally, η is the ratio between the maximum power (PMPP) to the power emitted by light in the active region of the solar cell (P_{light}).

$$\eta = \frac{P_{MPP}}{P_{light}} = \frac{P_{MPP}}{I \times A} = \frac{I_{SC} \times V_{OC} \times FF}{I \times A}$$
 (3)

3. Results

3.1 X-ray Diffraction Test

Figure 1 depicts the glass phase structure of the FTO-deposited glass phase determined by X-ray diffraction (XRD) after being treated with TiO₂ and/or TiCl₄. The anatase phase and the rutile phase of TiO₂ can be identified by all of the diffraction peaks. The peaks of TiO₂ in the rutile phase were more precise after TiCl₄ treatment than they were before. This is due to the fact that some anatase phase TiO₂ undergoes rutile phase TiO₂ transform following 500°C heat treatment.

The previous research shows that the mixture of TiO₂ anatase and TiO₂ rutile results in greater efficiency than using either of these materials alone. After pre-coating TiCl₄, the TiO₂ structure had no discernible impact. The angle of 26,836° at which the highest intensity value is found has a D value of 3.31947 18.4, as shown in Table 1.

XRD patterns with nano-TiO₂ and without nano-TiO₂ were shown in the rutile and anatase phases. With nano-TiO₂, the XRD pattern shows strong diffraction peaks at 27°, 36° and 55° indicating TiO₂ in the rutile phase. On the other hand, in the absence of nano-TiO₂, the XRD pattern exhibited strong diffraction peaks at 25° and 48° indicating TiO₂ in the anatase phase. All of the peaks are quite well in agreement with spectrum standards (JCPDS no.: 88-1175 and 84-1286). From Figure, it is shown that the peak diffraction pattern of TiO₂ intensity increases in proportion to the increasing particle size. The results showed that the nano-TiO₂ powder consisted of irregular polycrystalline. The presence of amorphism reveals a broad pattern of low intensity; However, the effect of the

amorphous material on the expansion of the XRD pattern on nanoTiO₂ was negligible. In the rutile phase, the d-spacing obtained was 0.301 nm, while the anatase d-spacing was 0.313 nm.

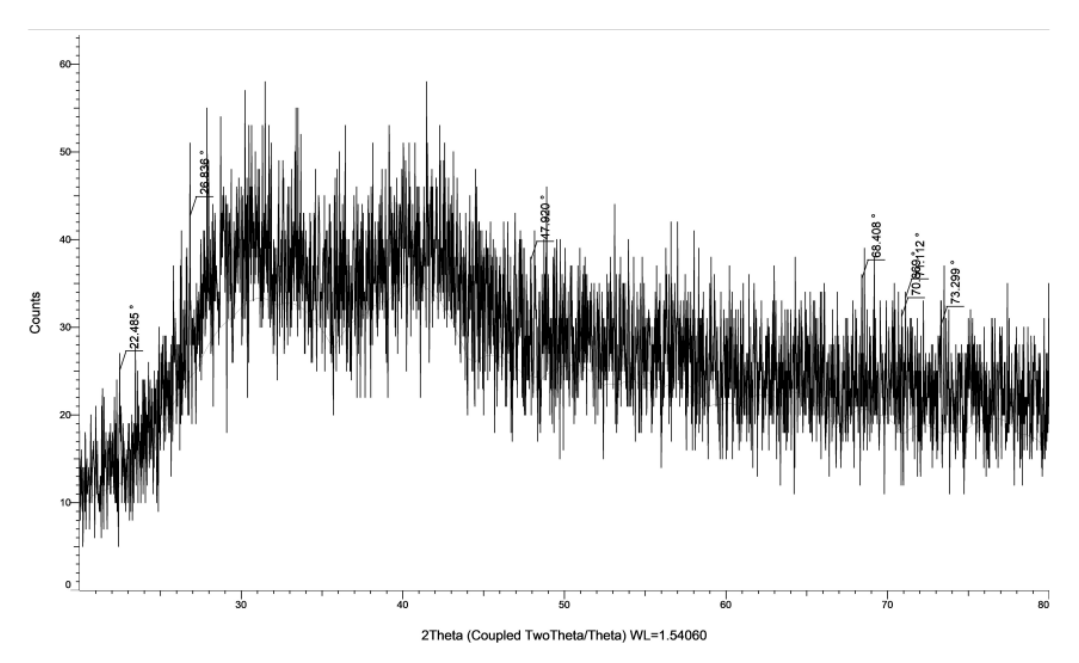


Figure 1. XRD test results

Table 1. XRD test peak point

Angle	D value	Net intensity	Gross intensity	Rail. intensity
22,485 °	3.95101 Å	13.0	25.1	70.2%
26,836 °	3.31947 Å	18.4	32.7	100.0%
47,920°	1.89683 Å	13.2	37.6	71.5%
68,408 °	1.37030 Å	14.9	35.5	80.9%
70,869°	1.32863 Å	13.2	31.2	71.6%
71,112 °	1.32468 Å	15.3	33.3	83.2%
73,299 °	1,29046 Å	12.3	30.2	66.8%

3.2 SEM Testing

Using an SEM device, the morphological structure of the semiconductor TiO_2 nanoparticles was observed. The SEM structure of the nanoparticles following $TiCl_4$ treatment is depicted in Figure 2. $TiCl_4$ was used to treat TiO_2 nanoparticles with different immersion times (10, 20, 30, 40, 50, and 60 mins) at a temperature of 70° C. Subgraphs (a) and (b) of Figure 2 show the SEM results after $TiCl_4$ treatment for 10 and 20mins respectively. The results demonstrate that there is still a lack of connectivity between the particles. There are still numerous gaps or spaces between these particles. The TiO_2 interparticle connection is better, as seen by the declining gaps between the particles in subgraphs (c) and (d) of Figure 2. These two figures show the SEM results after $TiCl_4$ treatment for 30 and 40 mins, respectively.

Moreover, subgraphs (e) and (f) of Figures 2 show the SEM results after TiCl₄ treatment for 50 and 60min, respectively. There is a good connectivity between TiO₂ particles, suggested by the small to zero gaps between particles. This is in line with earlier research, which indicates that the connection between semiconductor particles can be impacted by TiCl₄ treatment [35]. The reason is that the hydrolysis of TiCl₄ produces the TiO₂ layer, increasing the semiconductor's surface area [35, 36]. The flow of electrons and dyes absorbed in semiconductors will increase with increased connection between particles and semiconductor surface area, pushing up the Jsc value and DSSC efficiency [36-38].

The gaps' location and sizes were determined using ImageJ. Table 2 displays the significant amount of the gap region that the TiO₂ nanoparticles semiconductor's SEM data contain. With the aid of the Image J program, the distance between particles and the size of the distance may be estimated. The smallest gap area measured after immersion for 60mins is 6.76%.

As shown in Figure 2, the longer the immersion time between the gaps or between the particles, the thicker the resulting TiO₂ layer. Due to the hydrolysis of TiCl₄, the formation of the TiO₂ layer will also increase the semiconductor surface area, which in turn affects the amount of dye absorption and DSSC efficiency [36, 39, 40].

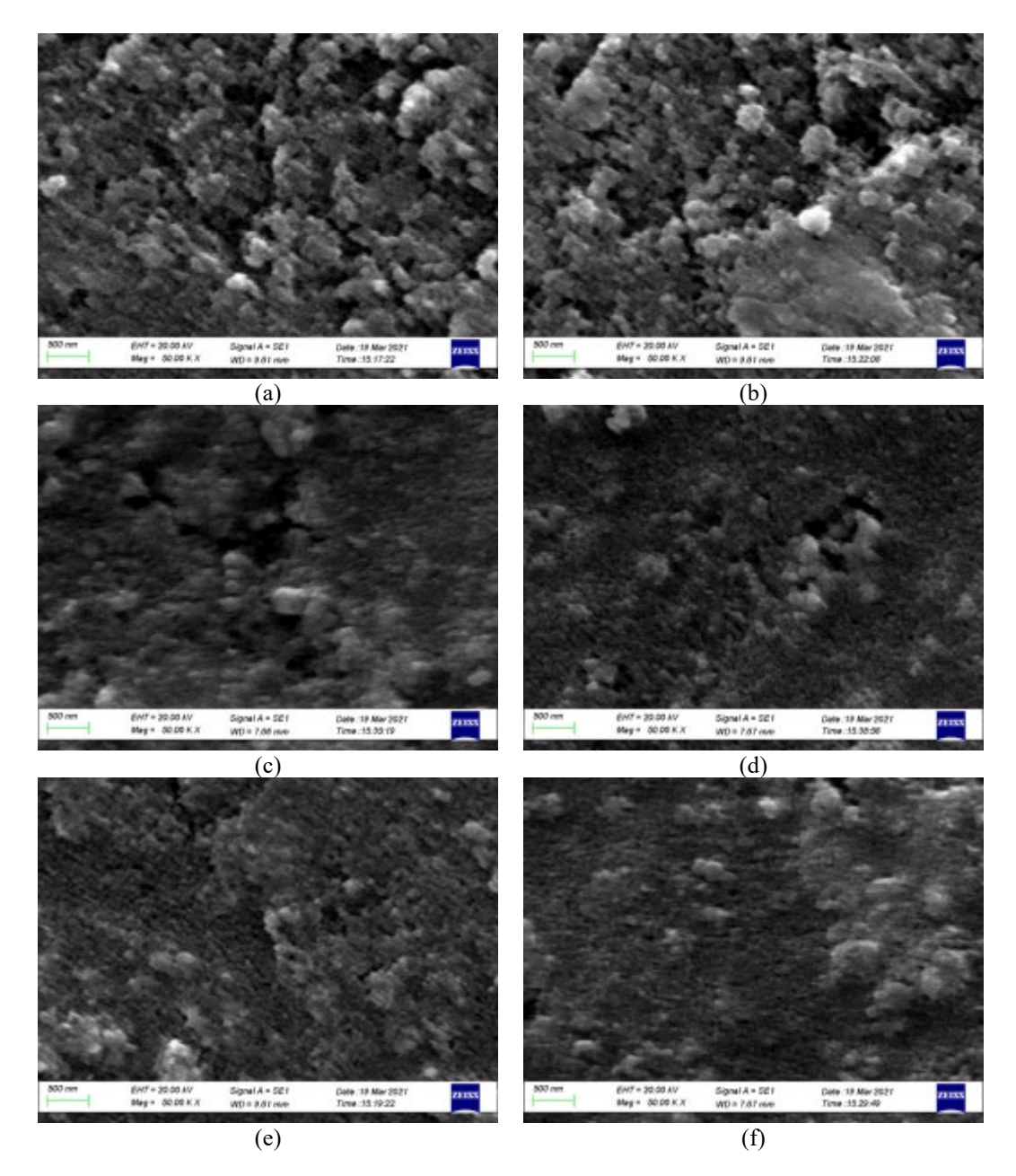


Figure 2. SEM results

Table 2. Percentage of gap area in semiconductors

Immersion time (mins)	Gap area (nm²)	Percentage (%)
10	2237308,727	11.14
20	2141125,133	10.66
30	2038865.56	10.15
40	1820467,571	9.07
50	1564363,779	7.79
60	1358361,544	6.76

3.3 Dye Loading Measurement

By separating the dye that has been absorbed into the semiconductor, the desorption method is used to calculate the amount of dye absorbed by the semiconductor. The dye-absorbing semiconductor was submerged in an alkaline solution for one hour to complete out the separation process. The solution will turn pink when the N719 dye dissolves, and the semiconductor will be colorless [40].

Figure 3 displays the Uv-Vis test results about the absorbance value against the wavelength. The absorbance values are 0.118%, 0.161%, 0.178%, 0.263%, 0.333%, and 0.370% for immersion times of 10, 20, 30, 40, 50, and

60 mins, respectively, at the wavelength range of 530-550 nm. Given that the length of the light path is 1 cm and the extrinsic molar value of the N719 solution is 14.100 M⁻¹.cm⁻¹, Figure 4 displays the dye loading value or the number of dye molecules absorbed. It can be seen that the dye loading was at its greatest with TiCl₄ treatment and a 60min immersion, at 20.9x10⁻⁸ mol/cm². This is due to the TiO₂ layer being formed, which expands the semiconductor surface area and raises the dye absorption potential [36, 40]. This is in accordance with the findings of the SEM test, which demonstrate that the formation of the TiO₂ layer increases with growing immersion duration and consequently raises the semiconductor's dye loading [36, 37].

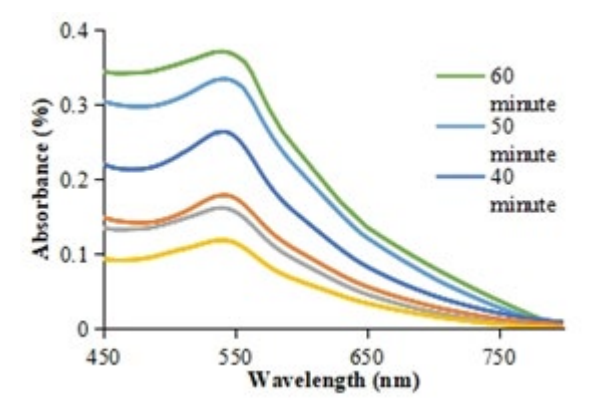


Figure 3. Variation of absorbance with wavelengths

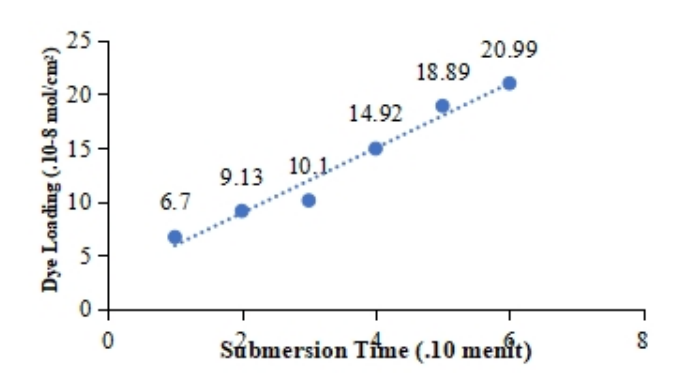


Figure 4. Dye loading value

Table 3. DSSC performance

Immersion time (minute)	Voc (V)	Jsc (mA / cm ²)	F (%)	η (%)
10	0.585	4,447	47.5	1,235
20	0.578	5,533	42.7	1,365
30	0.562	6,341	45.0	1,607
40	0.558	7,854	45.8	2,008
50	0.559	8,387	44.6	2,070
60	0.569	8,963	43.3	2,208

Table 3 lists the metrics of DSSC performance, including Jsc, Voc, FF, and η . Figure 5 shows the current density against voltage. The results of diesel test simulator are placed under a light intensity of 1000 W/m². DSSC with TiCl₄ treatment for 60 mins obtained the highest efficiency.

Table 3 shows how the DSSC performed with the changing immersion time of TiCl₄ treatment. As can be seen in Table 3, the Jsc of DSSC increased with the immersion time. This is because, the longer the immersion time, the better the connectivity between TiO₂ semiconductor particles, and the faster the electrons flow [38]. Apart from connectivity, the Jsc of the DSSC is also influenced by the amount of dye that the TiO₂ semiconductor can absorb. Previous research shows that the performance of the DSSC will increase in direct proportion to how much dye the semiconductor can absorb [37]. Consequently, the 60min-immersion period has the highest dye loading value, and the highest efficiency of 2.208%.

Figure 5 shows that the Jsc of the DSSC grew while the Voc value, which ranged from 0.6 to 0.7 V, did not changed significantly. This is partly due to the use of materials. Because the Voc of the DSSC is directly proportional to the bandgap of the semiconductor, semiconductors have the same bandgap values [9].

This study finds that DSSC efficiency rises as immersion time in TiCl₄ treatment increases. This correlation is significantly affected by the growth of Jsc. The increase of Jsc is attributable to the formation of a TiO₂ layer during the TiCl₄ treatment, which can promote particle connection and increase semiconductor surface area [36, 38, 40]. The TiO₂ semiconductor will transfer electrons faster due to the increased particle connection [36]. Additionally, the Jsc value will rise as a result of the increased semiconductor surface area due to an increase in dye loading value [35, 38, 39].

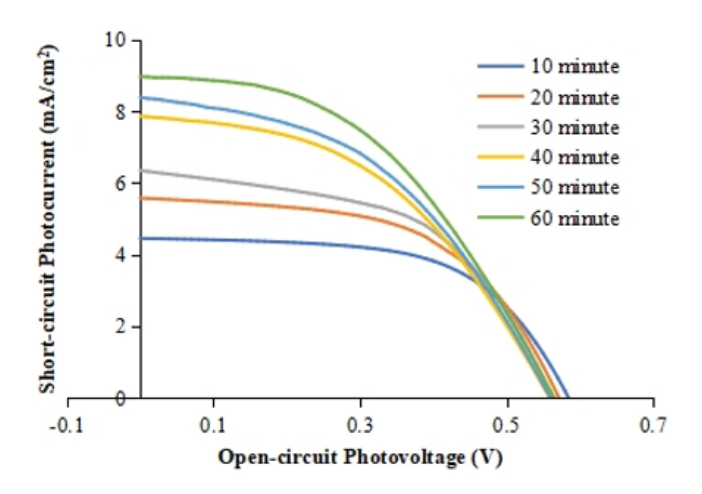


Figure 5. Graph IV

4. Conclusions

This paper successfully researches the production of DSSC double-layer TiO_2/ZnO with $TiCl_4$ treatment on TiO_2 nanoparticle semiconductors, when the immersion time varies. The results show that the TiO_2 semiconductor's connection between its particles and the amount of dye it can absorb will both grow when the immersion time of $TiCl_4$ treatment is extended. Due to an increase in electron production and transport, the Jsc and the efficiency of DSSC will both rise. The immersion time, which is set as 10, 20, 30, 40, 50, and 60mins, led to some variations. For DSSC efficiency, the highest value was achieved by the DSSC treated with $TiCl_4$ with a soaking time of 60 mins. This improves the efficiency by 2.208%. The best Voc, Jsc and FF values were 0.569 V, $8,963 \text{ mA/cm}^2$, and 43.3%, respectively. The immersion time was limited to 60min to ensure the measurement accuracy and speed up the analysis.

Funding

This work was partially supported by a PDUPT grant from the Ministry of Research, Technology, and Higher Education, the Republic of Indonesia (Grant no.: 719 / UN27.21 / PN / 2020 for FY 2021).

Data Availability

The data used to support the findings of this study are available from the corresponding author upon request.

Conflicts of Interest

The authors declare that they have no conflicts of interest.

REFERENCES

- [1] M. Wasfi, "Solar energy and photovoltaic systems," J. Sel. Area Renew. Sustain. Energ., vol. 2011, 2011.
- [2] S. Dubey, J. N. Sarvaiya, and B. Seshadri, "Temperature-dependent photovoltaic (PV) efficiency and its effect on PV production in the world A review," *Energy Procedia*, vol. 33, no. 3, pp. 311-321, 2013. https://doi.org/10.1016/j.egypro.2013.05.072.
- [3] M. Grätzel, "Dye-sensitized solar cells," *J. Photochem. Photobiol. C. Photochem. Rev.*, vol. 4, no. 2, pp. 145-153, 2003. https://doi.org/10.1016/S1389-5567(03)00026-1.
- [4] L. L. Tobin, T. O'Reilly, D. Zerulla, and J. T. Sheridan, "Characterizing dye-sensitized solar cells," *Optik Stuttg.*, vol. 122, pp. 1225-1230, 2011. https://doi.org/10.1016/j.ijleo.2010.07.028.
- [5] T. Marimuthu, N. Anandhan, and R. Thangamuthu, "Electrochemical synthesis of one-dimensional ZnO

- nanostructures on ZnO seed layer for DSSC applications," *Appl. Surf Sci.*, vol. 428, pp. 385-394, 2018. https://doi.org/10.1016/j.apsusc.2017.09.116.
- [6] M. K. Hossain, M. F. Pervez, M. N. H. Mia, A. A. Mortuza, M. S. Rahaman, M. Karim, J. M. Islam, F. Ahmed, and M. Khan, "Effect of dye extracting solvents and sensitization time on the photovoltaic performance of natural dye-sensitized solar cells," *Results. Phys.*, vol. 7, pp. 1516-1523, 2017. https://doi.org/10.1016/j.rinp.2017.04.011.
- [7] E. G. Galindo, M. J. Ariza, F. J. De Las Nieves, and M. J. García-Salinas, "Effects of multilayer coating and calcination procedures on dye-sensitized solar cell semiconductor photoelectrodes morphology," *Thin. Solid Films*, vol. 590, pp. 230-240, 2015. https://doi.org/10.1016/j.tsf.2015.07.078.
- [8] Y. Ooyama and Y. Harima, "Photophysical and electrochemical properties, and molecular structures of organic dyes for dye-sensitized solar cells," *ChemPhysChem*, vol. 13, no. 18, pp. 4032-4080, 2012. https://doi.org/10.1002/cphc.201200218.
- [9] C. C. Raj and R. Prasanth, "A critical review of recent developments in nanomaterials for photoelectrodes in dye-sensitized solar cells," *J. Power Sources*, vol. 317, pp. 120-132, 2016. https://doi.org/10.1016/j.jpowsour.2016.03.016.
- [10] H. Chang and Y. J. Lo, "Pomegranate leaves and mulberry fruit as natural sensitizers for dye-sensitized solar cells," *Sol. Energy*, vol. 84, no. 10, pp. 1833-1837, 2010. https://doi.org/10.1016/j.solener.2010.07.009.
- [11] R. Kumar, A. Umar, G. Kumar, H. S. Nalwa, A. Kumar, and M. S. Akhtar, "Zinc oxide nanostructure-based dye-sensitized solar cells," *J. Mater. Sci.*, vol. 52, no. 4743-95, 2017. https://doi.org/10.1007/s10853-016-0668-z.
- [12] Z. Arifin, S. Hadi, S. Suyitno, A. R. Prabowo, and S. D. Prasetyo, "Characterization of ZnO nanofiber on double-layer dye-sensitized solar cells using direct deposition method," *Period the Quim.*, vol. 17, no. 36, pp. 263-277, 2020. https://doi.org/10.52571/ptq.v17.n36.2020.278_periodico36_pgs_263_277.pdf.
- [13] A. Hegazy, N. Kinadjian, B. Sadeghimakki, S. Sivoththaman, N. K. Allam, and E. Prouzet, "TiO₂ nanoparticles optimized for photoanodes tested in large area Dye-sensitized solar cells (DSSC)," *Sol. Energy Mater. Sol. Cells*, vol. 153, pp. 108-116, 2016. https://doi.org/10.1016/j.solmat.2016.04.004.
- [14] G. Kanimozhi, S. Vinoth, H. Kumar, E. S. Srinadhu, and N. Satyanarayana, "Electrospun nanocomposite Ag-ZnO nanofibrous photoanode for better performance of dye-sensitized solar cells," *J. Electron. Mater.*, vol. 48, pp. 4389-4399, 2019. https://doi.org/10.1007/s11664-019-07199-2.
- [15] Z. Arifin, S. Soeparman, D. Widhiyanuriyawan, A. Purwanto, and D. Dharmanto, "Synthesis, characterization, and fabrication of hollow fibers of Zn-doped TiO₂ for dye-sensitized solar cells," *J. Eng. Sci. Technol.*, vol. 12, no. 5, pp. 1227-1239, 2022.
- [16] M. Yang, B. Dong, X. Yang, W. Xiang, Z. Ye, E. Wang, L. Wan, L. Zhao, and S. Wang, "TiO₂ nanoparticle/nanofiber-ZnO photoanode to enhance the efficiency of dye-sensitized solar cells," *RSC Adv.*, vol. 7, pp. 41738-44, 2017. https://doi.org/10.1039/c7ra07644d.
- [17] Z. Arifin, A. S. Ahmad, and T. S. Argatya, "Optimization parameters and synthesis of fluorine-doped tin oxide for dye-sensitized solar cells," *Appl. Mech. Mater.*, vol. 575, pp. 689-695, 2014. http://dx.doi.org/10.4028/www.scientific.net/AMM.575.689.
- [18] D. Rangel, J. C. Gallegos, S. Vargas, F. García, and R. Rodríguez, "Optimized dye-sensitized solar cells: A comparative study with different dyes, mordants and construction parameters," *Results Phys.*, vol. 12, pp. 2026-2037, 2019. https://doi.org/10.1016/j.rinp.2019.01.096.
- [19] T. Suprayogi, M. Z. Masrul, M. Diantoro, A. Taufiq, A. Fuad, and A. Hidayat, "The effect of annealing temperature of ZnO compact layer and TiO2 mesoporous on photo-supercapacitor performance," *IOP Conf. Ser. Mater. Sci. Eng.*, vol. 515, Article ID: 012006, 2019. https://doi.org/10.1088/1757-899X/515/1/012006.
- [20] Y. H. Lin, Y. C. Wu, and B. Y. Lai, "Collection efficiency enhancement of injected electrons in dyesensitized solar cells with a Ti interfacial layer and TiCl₄ treatment," *Int J. Electrochem Sci.*, vol. 7, no. 10, pp. 9478-87, 2012.
- [21] A. Sedghi and H. N. Miankushki, "Influence of TiCl₄ treatment on structure and performance of dyesensitized solar cells," *Jpn. J. Appl. Phys.*, vol. 52, no. 7, pp. 5002-5002, 2013. https://doi.org/10.7567/JJAP.52.075002.
- [22] V. Martina and A. G. Agrios, "Blocking layers for nanocomposite photoanodes in dye-sensitized solar cells: Comparison of atomic layer deposition and TiCl₄ treatment," *Thin. Solid Films*, vol. 598, pp. 54-59, 2016. https://doi.org/10.1016/j.tsf.2015.11.054.
- [23] S. G. Adhikari, A. Shamsaldeen, and G. G. Andersson, "The effect of TiCl₄ treatment on the performance of dye-sensitized solar cells," *J. Chem. Phys.*, vol. 151, Article ID: 164704, 2019. https://doi.org/10.1063/1.5125996.
- [24] F. Kabir, S. Nazmus Sakib, S. Shehab Uddin, E. Tawsif Efaz, and M. T. Farhan Himel, "Enhance cell performance of DSSC by dye mixture, carbon nanotube, and post TiCl₄ treatment along with degradation study," *Sustain. Energy Technol. Assessments*, vol. 35, pp. 298-307, 2019. https://doi.org/10.1016/j.seta.2019.07.011.

- [25] N. F. M. Sharif, S. Shafie, A. M. Z. A. Kadir, W. Z. W. Hasan, M. N. Mustafa, and B. Samaila, "The effect of titanium (IV) chloride surface treatment to enhance charge transport and performance of the dye-sensitized solar cell," *Results Phys.*, vol. 15, Article ID: 102725, 2019. https://doi.org/10.1016/j.rinp.2019.102725.
- [26] M. Mojaddami, Z. Andaji Garmaroudi, M. R. Mohammadi, and H. R. Madaah Hosseini, "Efficient dyesensitized solar cells based on TiO₂ nanoparticles and skin-like nanotubes: Effect of arrangement modes of the layers and TiCl₄ treatment," *J. Taiwan Inst. Chem. Eng.*, vol. 61, pp. 138-146, 2016. https://doi.org/10.1016/j.jtice.2015.12.004.
- [27] N. G. Park, J. van de Lagemaat, and A. J. Frank, "Comparison of dye-sensitized rutile- and anatase-based TiO₂ solar cells," *J. Phys. Chem. B*, vol. 104, no. 38, pp. 8989-94, 2000. https://doi.org/10.1021/jp9943651.
- [28] M. Mojaddami, M. R. Mohammadi, and H. R. Madaah Hosseini, "Improved efficiency of dye-sensitized solar cells based on a single layer deposition of skein-like TiO₂ nanotubes," *J. Am. Ceram. Soc.*, vol. 97, no. 9, 2014. https://doi.org/https://doi.org/10.1111/jace.13043.
- [29] H. Yu, B. Xue, P. Liu, J. Qiu, W. Wen, S. Zhang, and H. J. Zhao, "High-performance nanoporous TiO₂/La₂O₃ hybrid photoanode for dye-sensitized solar cells," *ACS Appl. Mater. Interfaces*, vol. 4, no. 3, pp. 1289-1294, 2012. https://doi.org/10.1021/am2015553
- [30] L. Li, S. Chen, C. Xu, Y. Zhao, N. G. Rudawski, and K. J. Ziegler, "Comparing electron recombination via interfacial modifications in dye-sensitized solar cells," *ACS Appl. Mater. Interfaces*, vol. 6, no. 23, pp. 20978-84, 2014. https://doi.org/10.1021/am505742y.
- [31] S. K. Park and Y. S. Han, "Efficient dye-sensitized solar cells with surface-modified photoelectrodes," *Sol. Energy*, vol. 110, pp. 260-267, 2014. https://doi.org/10.1016/j.solener.2014.09.019.
- [32] K. Balachandran, R. Venkatesh, R. Sivaraj, K. V. Hemalatha, and R. Mariappan, "Enhancing power conversion efficiency of DSSC by doping SiO₂ in TiO₂ photoanodes," *Mater. Sci. Semicond Process.*, vol. 35, pp. 59-65, 2015. https://doi.org/10.1016/j.mssp.2015.02.071.
- [33] S. W. Lee, K. S. Ahn, K. Zhu, N. R. Neale, and A. J. Frank, "Effects of TiCl4 treatment of nanoporous TiO2 films on morphology, light harvesting, and charge-carrier dynamics in dye-sensitized solar cells," *J. Phys. Chem. C*, vol. 116, no. 40, pp. 21285-21290, 2012. https://doi.org/10.1021/jp3079887.
- [34] A. M. Shahrul, M. Y. Syarifah Adilah, R. Radzali, M. F. Malek, I. S. Isa, M. Rusop, N. S. Damanhuri, and M. H. Abdullah, "Low-cost coagulation treatment of dye sensitizer for improved time immersion of dye-sensitized solar cells (DSSC)," *Microelectron. Eng.*, vol. 262, Article ID: 111832, 2022. https://doi.org/10.1016/j.mee.2022.111832.
- [35] Z. Arifin, S. Hadi, H. N. Jati, and S. D. Suyitno, "Effect of electrospinning distance to fabricate ZnO nanofiber as photoanode of dye-sensitized solar cells," *AIP Conf. Proc.* 2020, vol. 2217, Article ID: 030095, 2020. https://doi.org/10.1063/5.0000705.
- [36] J. Li, H. Zhang, W. Wang, Y. Qian, and Z. Li, "Improved performance of dye-sensitized solar cell based on TiO₂ photoanode with FTO glass and film treated by TiCl₄," *Phys B Condens Matter.*, vol. 500, pp. 48-52, 2016. https://doi.org/10.1016/j.physb.2016.07.021.
- [37] P. Charoensirithavorn, Y. Ogomi, T. Sagawa, S. Hayase, and S. Yoshikawa, "Improvement of dye-sensitized solar cell through TiCl₄-Treated TiO₂ nanotube arrays," *J. Electrochem. Soc.*, vol. 157, no. 3, pp. B354-B354, 2016. https://doi.org/10.1149/1.3280229.
- [38] H. Choi, C. Nahm, J. Kim, J. Moon, S. Nam, D. R. Jung, and P. Byungwoo, "The effect of TiCl₄-treated TiO₂ compact layer on the performance of the dye-sensitized solar cell," *Curr. Appl. Phys.*, vol. 12, no. 3, pp. 737-741, 2012. https://doi.org/10.1016/j.cap.2011.10.011.
- [39] S. Ito, T. N. Murakami, P. Comte, P. Liska, C. Grätzel, M. K. Nazeeruddin, and M. Gratzel, "Fabrication of thin-film dye-sensitized solar cells with solar to electric power conversion efficiency over 10%," *Thin. Solid Films*, vol. 516, no. 14, pp. 4613-4619, 2008. https://doi.org/10.1016/j.tsf.2007.05.090.
- [40] F. A. S. Lima, I. F. Vasconcelos, and M. Lira-Cantu, "Electrochemically synthesized mesoporous thin films of ZnO for highly efficient dye-sensitized solar cells," *Ceram. Int*, vol. 41, no. 8, pp. 9314-9320, 2015. https://doi.org/10.1016/j.ceramint.2015.03.271.